Pergamon

Carbon, Vol. 33, No. 7, pp. 979–988, 1995
Copyright © 1995 Elsevier Science Ltd
Printed in Great Britain. All rights reserved
0008-6223/95 $9.50 + .00

0008-6223(95)00026-7

NANOPARTICLES AND FILLED NANOCAPSULES

YAHACHI SAITO
Department of Electrical and Electronic Engineering, Mie University, Tsu 514 Japan

(*Received* 11 *October* 1994; *accepted in revised form* 10 *February* 1995)

Abstract—Encapsulation of foreign materials within a hollow graphitic cage was carried out for rare-earth and iron-group metals by using an electric arc discharge. The rare-earth metals with low vapor pressures, Sc, Y, La, Ce, Pr, Nd, Gd, Tb, Dy, Ho, Er, Tm, and Lu, were encapsulated in the form of carbides, whereas volatile Sm, Eu, and Yb metals were not. For iron-group metals, particles in metallic phases (α-Fe, γ-Fe; hcp-Co, fcc-Co; fcc-Ni) and in a carbide phase (M_3C, M = Fe, Co, Ni) were wrapped in graphitic carbon. The excellent protective nature of the outer graphitic cages against oxidation of the inner materials was demonstrated. In addition to the wrapped nanoparticles, exotic carbon materials with hollow structures, such as single-wall nanotubes, bamboo-shaped tubes, and nanochains, were produced by using transition metals as catalysts.

Key Words—Nanoparticles, nanocapsules, rare-earth elements, iron, cobalt, nickel.

1. INTRODUCTION

The carbon-arc plasma of extremely high temperatures and the presence of an electric field near the electrodes play important roles in the formation of nanotubes[1,2] and nanoparticles[3]. A nanoparticle is made up of concentric layers of closed graphitic sheets, leaving a nanoscale cavity in its center. Nanoparticles are also called nanopolyhedra because of their polyhedral shape, and are sometimes dubbed as nanoballs because of their hollow structure.

When metal-loaded graphite is evaporated by arc discharge under an inactive gas atmosphere, a wide range of composite materials (e.g., filled nanocapsules, single-wall tubes, and metallofullerenes, R@C_{82}, where R = La, Y, Sc,[4–6]) are synthesized. Nanocapsules filled with LaC_2 crystallites were discovered in carbonaceous deposits grown on an electrode by Ruoff *et al.*[7] and Tomita *et al.*[8]. Although rare-earth carbides are hygroscopic and readily hydrolyze in air, the carbides nesting in the capsules did not degrade even after a year of exposure to air. Not only rare-earth elements but also 3*d*-transition metals, such as iron, cobalt, and nickel, have been encapsulated by the arc method. Elements that are found, so far, to be incapsulated in graphitic cages are shown in Table 1.

In addition to nanocapsules filled with metals and carbides, various exotic carbon materials with hollow structures, such as single-wall (SW) tubes[9,10], bamboo-shaped tubes, and nanochains[11], are produced by using transition metals as catalysts.

In this paper, our present knowledge and understanding with regard to nanoparticles, filled nanocapsules, and the related carbon materials are described.

2. PREPARATION PROCEDURES

Filled nanocapsules, as well as hollow nanoparticles, are synthesized by the dc arc-evaporation method that is commonly used to synthesize fullerenes and nanotubes. When a pure graphite rod (anode) is evaporated in an atmosphere of noble gas, macroscopic quantities of hollow nanoparticles and multi-wall nanotubes are produced on the top end of a cathode. When a metal-packed graphite anode is evaporated, filled nanocapsules and other exotic carbon materials with hollow structures (e.g., "bamboo"-shaped tubes, nanochains, and single-wall (SW) tubes) are also synthesized. Details of the preparation procedures are described elsewhere[8,11,12].

3. NANOPARTICLES

Nanoparticles grow together with multi-wall nanotubes in the inner core of a carbonaceous deposit formed on the top of the cathode. The size of nanoparticles falls in a range from a few to several tens of nanometers, being roughly the same as the outer diameters of multi-wall nanotubes. High-resolution TEM (transmission electron microscopy) observations reveal that polyhedral particles are made up of concentric graphitic sheets, as shown in Fig. 1. The closed polyhedral morphology is brought about by well-developed graphitic layers that are flat except at the corners and edges of the polyhedra. When a pentagon is introduced into a graphene sheet, the sheet curves positively and the strain in the network structure is localized around the pentagon. The closed graphitic cages produced by the introduction of 12 pentagons will exhibit polyhedral shapes, at the corners of which the pentagons are located. The overall shapes of the polyhedra depend on how the 12 pentagons are located. Carbon nanoparticles actually synthesized are multilayered, like a Russian doll. Consequently, nanoparticles may also be called gigantic multilayered fullerenes or gigantic hyper-fullerenes[13].

The spacings between the layers (d_{002}) measured by selected area electron diffraction were in a range of 0.34 to 0.35 nm[3]. X-ray diffraction (XRD) of the cathode deposit, including nanoparticles and nano-

Table 1. Formation of filled nanocapsules. Elements in shadowed boxes are those which were encapsulated so far. M and C under the chemical symbols represent that the trapped elements are in metallic and carbide phases, respectively. Numbers above the symbols show references.

Li	Be											B	C	N	O	F	Ne
Na	Mg											Al	Si	P	S	Cl	Ar
K	Ca	11, 21 Sc C	Ti	47 V C	Cr C	Mn	11, 29 Fe M,C	11 Co M,C	11, 34 Ni M,C	Cu M	Zn	Ga	Ge	As	Se	Br	Kr
Rb	Sr	12, 23 Y C	47 Zr C	Nb	Mo C	Tc	Ru	Rh	Pd	Ag	Cd	In	Sn	Sb	Te	I	Xe
Cs	Ba	lanthanides	Hf	48 Ta C	W	Re	Os	Ir	Pt	49 Au M	Hg	Tl	Pb	Bi	Po	At	Rn
Fr	Ra	Ac	25 Th C	Pa	26 U C	Np	Pu	Am	Cm	Bk	Cf	Es	Fm	Md	No	Lr	

7, 8 La C	11, 12 Ce C	11, 12 Pr C	11, 12 Nd C	Pm	Sm	Eu	11, 12 Gd C	11, 12 Tb C	11, 12 Dy C	11, 12 Ho C	11, 12 Er C	12 Tm C	Yb	11, 12 Lu C

tubes, gave $d_{002} = 0.344$ nm[14], being consistent with the result of electron diffraction. The interlayer spacing is wider by a few percent than that of the ideal graphite crystal (0.3354 nm). The wide interplanar spacing is characteristic of the turbostratic graphite[15].

Figure 2 illustrates a proposed growth process[3] of a polyhedral nanoparticle, along with a nanotube. First, carbon neutrals (C and C_2) and ions (C^+)[16] deposit, and then coagulate with each other to form small clusters on the surface of the cathode. Through an accretion of carbon atoms and coalescence between clusters, clusters grow up to particles with the size finally observed. The structure of the particles at this stage may be "quasi-liquid" or amorphous with high structural fluidity because of the high temperature ($\approx$3500 K)[17] of the electrode and ion bombardment. Ion bombardment onto the electrode surface seems to be important for the growth of nanoparticles, as well as tubes. The voltage applied between the electrodes is concentrated within thin layers just above the surface of the respective electrodes because the arc plasma is electrically conductive, and thereby little drop in voltage occurs in a plasma pillar. Near a cathode, the voltage drop of approximately 10 V occurs in a thin layer of 10^{-3} to 10^{-4} cm from the electrode surface[18]. Therefore, C^+ ions with an average kinetic energy of ~10 eV bombard the carbon particles and enhance the fluidity of particles. The kinetic energy of the carbon ions seems to affect the structure of deposited carbon. It is reported that tetrahedrally coordinated amorphous carbon films, exhibiting mechanical properties similar to diamond, have been grown by deposition of carbon ions with energies between 15 and 70 eV[19]. This energy is slightly higher than the present case, indicating that the structure of the deposited material is sensitive to the energy of the impinging carbon ions.

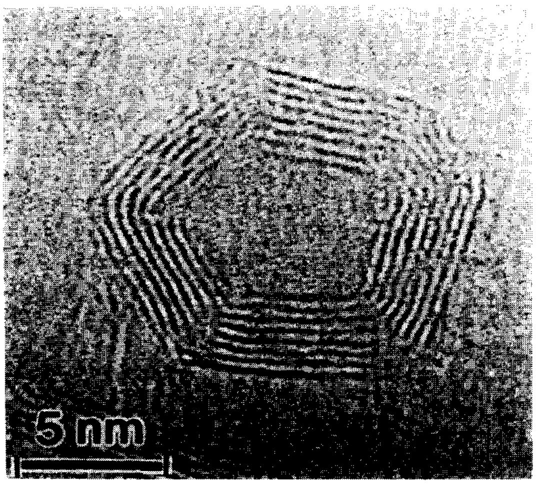

Fig. 1. TEM picture of a typical nanoparticle.

The vapor deposition and ion bombardment onto quasi-liquid particles will continue until the particles are shadowed by the growth of tubes and other particles surrounding them and, then, graphitization occurs. Because the cooling goes on from the surface to the center of the particle, the graphitization initiates on the external surface of the particle and progresses toward its center. The internal layers grow, keeping

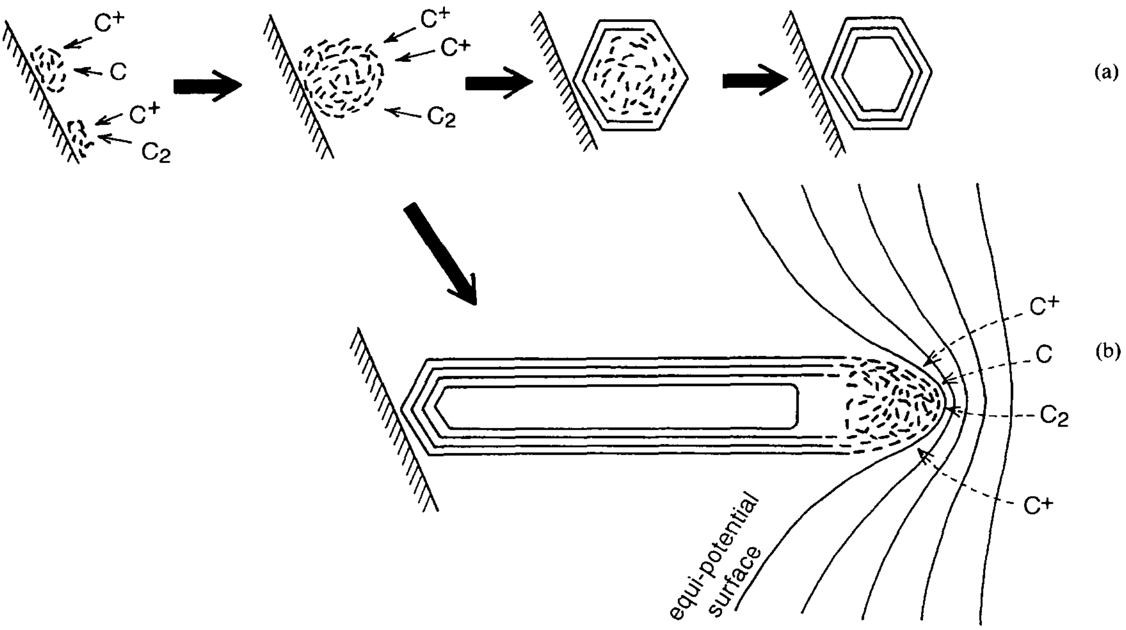

Fig. 2. A model of growth processes for (a) a hollow nanoparticle and, (b) a nanotube; curved lines depicted around the tube tip show schematically equal potential surfaces.

their planes parallel to the external layer. The flat planes of the particle consist of nets of six-member rings, while five-member rings may be located at the corners of the polyhedra. The closed structure containing pentagonal rings diminishes dangling bonds and lowers the total energy of a particle. Because the density of highly graphitized carbon ($\approx$ 2.2 g/cm^3) is higher than that of amorphous carbon (1.3–1.5 g/cm^3), a pore will be left inevitably in the center of a particle after graphitization. In fact, the corresponding cavities are observed in the centers of nanoparticles.

4. FILLED NANOCAPSULES

4.1 *Rare earths*

4.1.1 *Structure and morphology.* Most of the rare-earth elements were encapsulated in multilayered graphitic cages, being in the form of single-domain carbides. The carbides encapsulated were in the phase of RC_2 (R stands for rare-earth elements) except for Sc, for which Sc_3C_4[20] was encapsulated[21].

A high-resolution TEM image of a nanocapsule encaging a single-domain YC_2 crystallite is shown in Fig. 3. In the outer shell, (002) fringes of graphitic layers with 0.34 nm spacing are observed and, in the core crystallite, lattice fringes with 0.307-nm spacing due to (002) planes of YC_2 are observed. The YC_2 nanocrystal partially fills the inner space of the nanocapsule, leaving a cavity inside. No intermediate phase was observed between the core crystallite and the graphitic shell. The external shapes of nanocapsules were polyhedral, like the nanoparticles discussed above, while the volume ratio of the inner space (including the volume of a core crystallite and a cavity) to the whole particle is greater for the stuffed nanocapsules than that for hollow nanoparticles. While the inner space within a hollow nanoparticle is only ~1% of the whole volume of the particle, that for a filled nanocapsule is 10 to 80% of the whole volume.

The lanthanides (from La to Lu) and yttrium form isomorphous dicarbides with a structure of the CaC_2 type (body-centered tetragonal). These lanthanide carbides are known to have conduction electrons (one

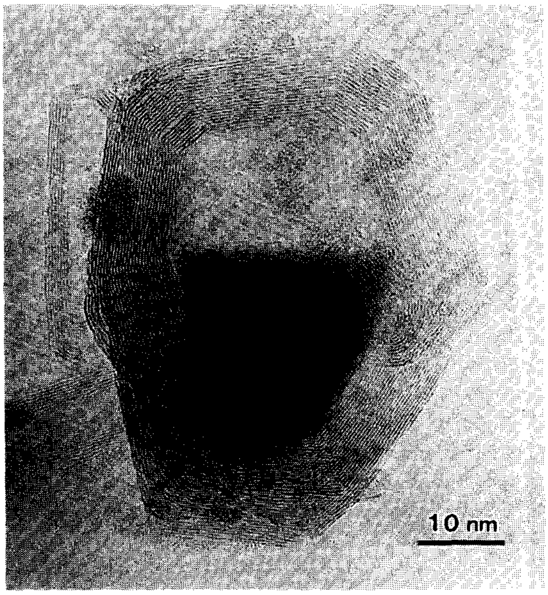

Fig. 3. TEM image of a YC_2 crystallite encapsulated in a nanocapsule.

electron per formula unit, RC_2)[22] (i.e., metallic electrical properties) though they are carbides. All the lanthanide carbides including YC_2 and Sc_3C_4 are hygroscopic; they quickly react with water in air and hydrolyze, emanating hydrogen and acetylene. Therefore, they usually have to be treated and stored in an inactive gas atmosphere or oil to avoid hydrolysis. However, the observation of intact dicarbides, even after exposure to air for over a year, shows the excellent airtight nature of nanocapsules, and supports the hypothesis that their structure is completely closed by introducing pentagons into graphitic sheets like fullerenes[23].

4.1.2 *Correlation between metal volatility and encapsulation.* A glance at Table 1 shows us that carbon nanocapsules stuffed with metal carbides are formed for most of the rare-earth metals, Sc, Y, La, Ce, Pr, Nd, Gd, Tb, Dy, Ho, Er, and Lu. Both TEM and XRD confirm the formation of encapsulated carbides for all the above elements. The structural and morphological features described above for Y are common to all the stuffed nanocapsules: the outer shell, being made up of concentric multilayered graphitic sheets, is polyhedral, and the inner space is partially filled with a single-crystalline carbide. It should be noted that the carbides entrapped in nanocapsules are those that have the highest content of carbon among the known carbides for the respective metal. This finding provides an important clue to understanding the growth mechanism of the filled nanocapsules (see below).

In an XRD profile from a Tm-C deposit, a few faint reflections that correspond to reflections from TmC_2 were observed[12]. Owing to the scarcity of TmC_2 particles, we have not yet obtained any TEM images of nanocapsules containing TmC_2. However, the observation of intact TmC_2 by XRD suggests that TmC_2 crystallites are protected in nanocapsules like the other rare-earth carbides.

For Sm, Eu, and Yb, on the other hand, nanocapsules containing carbides were not found in the cathode deposit by either TEM or XRD. To see where these elements went, the soot particles deposited on the walls of the reaction chamber was investigated for Sm. XRD of the soot produced from Sm_2O_3/C composite anodes showed the presence of oxide (Sm_2O_3) and a small amount of carbide (SmC_2). TEM, on the other hand, revealed that Sm oxides were naked, while Sm carbides were embedded in flocks of amorphous carbon[12]. The size of these compound particles was in a range from 10 to 50 nm. However, no polyhedral nanocapsules encaging Sm carbides were found so far.

Figure 4 shows vapor pressure curves of rare-earth metals[24], clearly showing that there is a wide gap between Tm and Dy in the vapor pressure-temperature curves and that the rare-earth elements are classified into two groups according to their volatility (viz., Sc, Y, La, Ce, Pr, Nd, Gd, Tb, Dy, Ho, Er, and Lu, non-volatile elements, and Sm, Eu, Tm, and Yb, volatile elements). Good correlation between the volatility and the encapsulation of metals was recently pointed out[12]; all the encapsulated elements belong to the group of non-volatile metals, and those not encapsulated, to the group of volatile ones with only one exception, Tm.

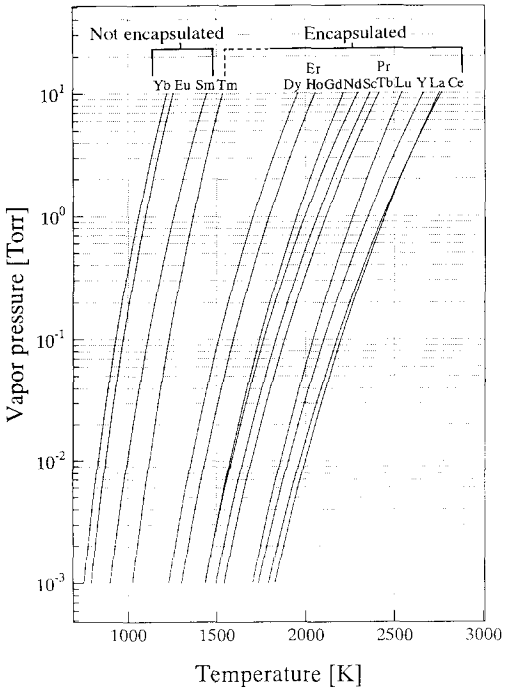

Fig. 4. Vapor pressure curves of rare-earth metals reproduced from the report of Honig[24]. Elements are distinguished by their vapor pressures. Sm, Eu, Tm, and Yb are volatile, and Sc, Y, La, Ce, Pr, Nd, Gd, Tb, Dy, Ho, Er, and Lu are non-volatile.

Although Tm is classified into the group of volatile metals, it has the lowest vapor pressure within this group and is next to the non-volatile group. This intermediary property of Tm in volatility may be responsible for the observation of trace amount of TmC_2. The vapor pressure of Tm suggests the upper limit of volatility of metals that can be encapsulated.

This correlation of volatility with encapsulation suggests the importance of the vapor pressure of metals for their encapsulation. In the synthesis of the stuffed nanocapsules, a metal-graphite composite was evaporated by arc heating, and the vapor was found to deposit on the cathode surface. A growth mechanism for the stuffed nanocapsules (see Fig. 5) has been proposed by Saito *et al.*[23] that explains the observed features of the capsules. According to the model, particles of metal-carbon alloy in a liquid state are first formed, and then the graphitic carbon segregates on the surface of the particles with the decrease of temperature. The outer graphitic carbon traps the metal-carbon alloy inside. The segregation of carbon continues until the composition of alloy reaches RC_2 ($R = Y$, La, ..., Lu) or Sc_2C_3, which equilibrates with graphite. The co-deposition of metal and carbon atoms on the cathode surface is indispensable for the formation of the stuffed nanocapsules. However, because the

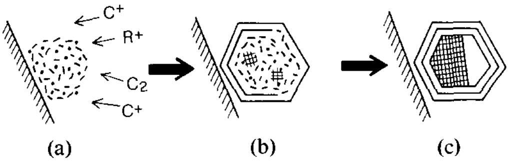

Fig. 5. A growth model of a nanocapsule partially filled with a crystallite of rare-earth carbide (RC_2 for R = Y, La, . . . , Lu; R_3C_4 for R = Sc): (a) R-C alloy particles, which may be in a liquid or quasi-liquid phase, are formed on the surface of a cathode; (b) solidification (graphitization) begins from the surface of a particle, and R-enriched liquid is left inside; (c) graphite cage outside equilibrates with RC_2 (or R_3C_4 for R = Sc) inside.

temperature of the cathode surface is as high as 3500 K, volatile metals do not deposit on a surface of such a high temperature, or else they re-evaporate immediately after they deposit. Alternatively, since the shank of an anode (away from the arc gap) is heated to a rather high temperature (e.g., 2000 K), volatile metals packed in the anode rod may evaporate from the shank into a gas phase before the metals are exposed to the high-temperature arc. For Sm, which was not encapsulated, its vapor pressure reaches as high as 1 atmosphere at 2000 K (see Fig. 4).

The criterion based on the vapor pressure holds for actinide; Th and U, being non-volatile (their vapor pressures are much lower than La), were recently found to be encapsulated in a form of dicarbide, ThC_2[25] and UC_2[26], like lanthanide.

It should be noted that rare-earth elements that form metallofullerenes[27] coincide with those that are encapsulated in nanocapsules. At present, it is not clear whether the good correlation between the metal volatility and the encapsulation found for both nanocapsules and metallofullerenes is simply a result of kinetics of vapor condensation, or reflects thermodynamic stability. From the viewpoint of formation kinetics, to form precursor clusters (transient clusters comprising carbon and metal atoms) of filled nanocapsules or metallofullerenes, metal and carbon have to condense simultaneously in a spatial region within an arc-reactor vessel (i.e., the two regions where metal and carbon condense have to overlap with each other spatially and chronologically). If a metal is volatile and its vapor pressure is too high compared with that of carbon, the metal vapor hardly condenses on the cathode or near the arc plasma region. Instead, it diffuses far away from the region where carbon condenses and, thereby, the formation of mixed precursor clusters scarcely occurs.

4.2 *Iron-group metals (Fe, Co, Ni)*

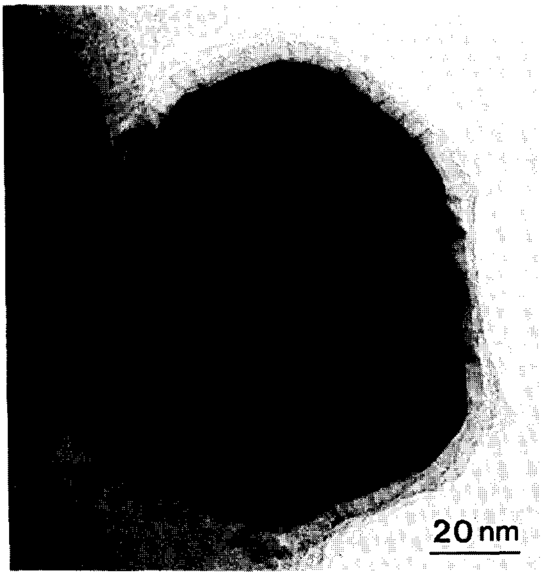

Fig. 6. TEM picture of an α-Fe particle grown in the cathode soot; the core crystallite is wrapped in graphitic carbon.

4.2.1 *Wrapped nanocrystals.* Metal crystallites covered with well-developed graphitic layers are found in soot-like material deposited on the outer surface of a cathode slag. Figure 6 shows a TEM picture of an α(bcc)-Fe particle grown in the cathode soot. Generally, iron crystallites in the α-Fe phase are faceted. The outer shell is uniform in thickness, and it usually consists of several to about 30 graphene layers[28]. Nanocapsules of the iron-group metals (Fe, Co, Ni) show structures and morphology different from those of rare-earth elements in the following ways. First, most of the core crystallites are in ordinary metallic phases (i.e., carbides are minor). The α-Fe, β(fcc)-Co and fcc-Ni are the major phases for the respective metals, and small amounts of γ(fcc)-Fe and α(hcp)-Co are also formed[11]. Carbides formed for the three metals were of the cementite phase (viz., Fe_3C, Co_3C, and Ni_3C). The quantity of carbides formed depends on the affinity of the metal toward carbon; iron forms the carbide most abundantly (about 20% of metal atoms are in the carbide phase)[29], nickel forms the least amount (on the order of 1%), and cobalt, intermediate between iron and nickel.

Secondly, the outer graphitic layers tightly surround the core crystallites without a gap for most of the particles, in contrast to the nanocapsules of rare-earth carbides, for which the capsules are polyhedral and have a cavity inside. The graphite layers wrapping iron (cobalt and nickel) particles bend to follow the curvature of the surface of a core crystallite. The graphitic sheets, for the most part, seem to be stacked parallel to each other one by one, but defect-like contrast suggesting dislocations, was observed[28], indicating that the outer carbon shell is made up of small domains of graphitic carbon stacked parallel to the surface of the core particle. The structure may be similar to that of graphitized carbon blacks, being composed of small segments of graphitic sheets stacked roughly parallel to the particle surface[30].

Magnetic properties of iron nanocrystals nested in carbon cages, which grew on the cathode deposit, have been studied by Hiura *et al.*[29]. Magnetization (*M-H*) curves showed that the coercive force, H_c, of this nanoscale encapsulated material at room temperature is about 80 Oe, larger than that of bulk α-Fe ($H_c \approx 1$ Oe). The particle sizes of iron studied (10 to 100 nm) and the large coercive force suggests that the magnetization process is dominated by the cooperative spin rotation of single domains. The saturation magnetization was 25 emu/g, being smaller than that for pure α-Fe (221.7 emu/g) because the measured sample contains a large amount of free carbon as well as wrapping graphite. For application, magnetic particles have to be extracted, and it is also necessary to control the size and composition of iron particles to obtain larger coercive force and magnetization.

Iron, cobalt, and nickel particles also grow in soot deposited on the chamber walls, but graphitic layers wrapping the metals are not so well-developed as those grown in the cathode soot. Figure 7 shows a TEM picture of iron particles grown in the chamber soot. They are nearly spherical in shape and are embedded in amorphous carbon globules. For some iron particles, lattice fringes (0.34–0.35 nm spacing) suggesting the presence of a few layers of graphene sheets between their surface and the outer amorphous carbon are observed, as indicated by arrows. The iron is predominantly in α-Fe phase, and minorities are in γ-Fe and Fe_3C phases. The iron particles in the chamber soot are smaller (3–10 nm) than those in the cathode soot. Much higher coercive force of 380 Oe and superparamagnetism were observed for the smaller iron nanocrystals grown in the chamber soot[31].

Majetich and coworkers have studied magnetic properties of carbon-coated Co[32], Gd_2C_3, and Ho_2C_3 nanocrystals[33] formed in the chamber soot. A brief account on the coated Co nanocrystals is given here. They extracted magnetic nanocrystals from the crude soot with a magnetic gradient field technique.

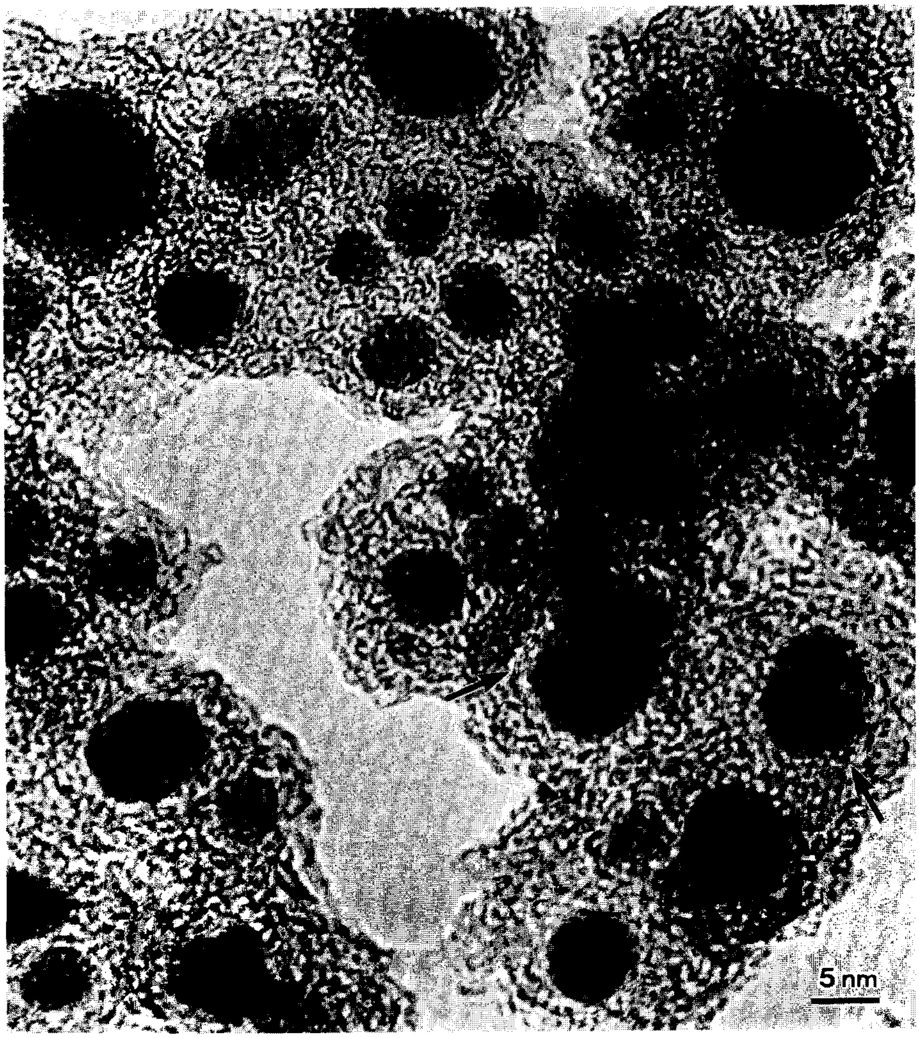

Fig. 7. TEM picture of iron nanocrystals collected from the chamber soot; nanocrystals are embedded in amorphous carbon globules. On the surface of some core crystals, a few fringes with 0.34–0.35 nm spacing suggesting the presence of graphitic layers are observed, as indicated by arrows.

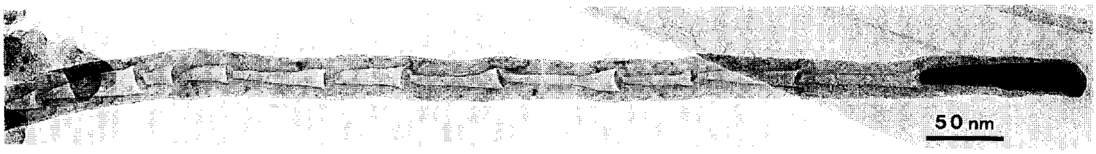

Fig. 8. TEM picture of a bamboo-shaped carbon tube.

The majority of Co nanocrystals (in the fcc phase) exist as nominally spherical particles with a 0.5–5 nm in radius. Hysteretic and temperature-dependent magnetic response, in randomly and magnetically aligned powder samples frozen in epoxy, revealed fine particle magnetism associated with single-domain Co particles. These single-domain particles exhibited superparamagnetic response with magnetic hysteresis observed only at temperatures below T_B (blocking temperature) $\approx$ 160 K.

4.2.2 *Bamboo-shaped tubes.* A carbon tube with a peculiar shape looking like "bamboo," produced by the arc evaporation of nickel-loaded graphite, is shown in Fig. 8. The tube consists of a linear chain of hollow compartments that are spaced at nearly equal separation from 50 to 100 nm. The outer diameter of the bamboo tubes is about 40 nm, and the length typically several μm. One end of the tube is capped with a needle-shaped nickel particle which is in the normal fcc phase, and the other end is empty. Walls of each compartment are made up by about 20 graphitic layers[34]. The shape of each compartment is quite similar to the needle-shape of the Ni particle at the tip, suggesting that the Ni particle was once at the cavities.

Figure 9 illustrates a growth process of the bamboo tubes. It is not clear whether the Ni particle at the tip was liquid or solid during the growth of the tube. We infer that the cone-shaped Ni was always at the tip and it was absorbing carbon vapor. The dissolved carbon diffused into the bottom of the Ni needle, and carbon segregated as graphite at the bottom and the side of the needle. After graphitic layers (about 20 layers) were formed, the Ni particle probably jumped out of the graphitic sheath to the top of the tube. The motive force of pushing out the Ni needle may be a stress accumulated in the graphitic sheath due to the segregation of carbon from the inside of the sheath.

The segregation process of graphite on the surface of a metal particle is similar to that proposed by Oberlin and Endo[35] for carbon fibers prepared by thermal decomposition of hydrocarbons. However, the lengthening of tubes goes on intermittently for the bamboo-shaped tubes, while the pyrolytic fibers grow continuously.

A piece of Ni metal was sometimes left in a compartment located in the middle of a bamboo tube, as shown in Fig. 10. The shape of the trapped metal is reminiscent of a drop of mercury left inside a glass capillary. The contact angle between the Ni metal and the inner wall of graphite is larger than 90° (measured angle is about 140°), indicating that the metal poorly wets the tube walls. Strong capillary action, anticipated in nanometer-sized cavities[36,37], does not seem to be enough to suck the metal into the tubes, at least for the present system[11,38].

4.2.3 *Nanochains.* Figure 11 shows a TEM picture of nanochains produced from a Ni/C composite anode[11]. The nanochains consist of spherical, hollow graphitic particles with outer diameters of 10–20 nm and inner diameters of several to 10 nm. A nanochain comprises a few tens of hollow particles that are linearly connected with each other. The inside of some particles is filled with a Ni particle, as seen in the figure. The morphology of each particle resembles that of graphitized carbon blacks, which are made up of many patches of small graphitic sheets piling up to form spherical shapes.

The chains of hollow carbon may be initially chains consisting of Ni (or carbide) particles covered with graphitic carbon. The chains lying on the hot surface of the cathode are heated, and Ni atoms evaporate through defects of the outer graphitic carbon because the vapor pressure of Ni is much higher than carbon. Thus, the carbon left forms hollow graphitic layers.

Seraphin *et al.*[39] reported that an arc evaporation of Fe/C composite anode also generated nanochains with similar morphology, described above.

4.2.4 *Single-wall tubes.* Following the synthesis studies of stuffed nanocapsules, single-wall (SW) tubes were discovered in 1993[9,10]. SW tubes are found in chamber soot when iron[9] and cobalt[10] were used as catalysts, and for nickel[11,40] they grow on the surface of the cathode slag. For iron catalyst,

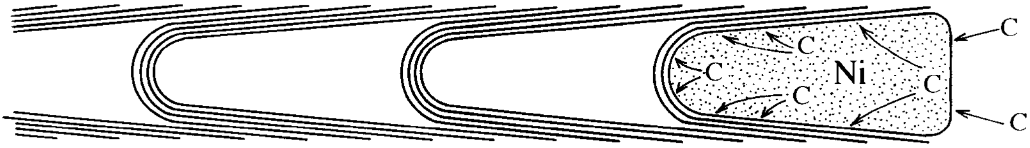

Fig. 9. Growth model of a bamboo tube.

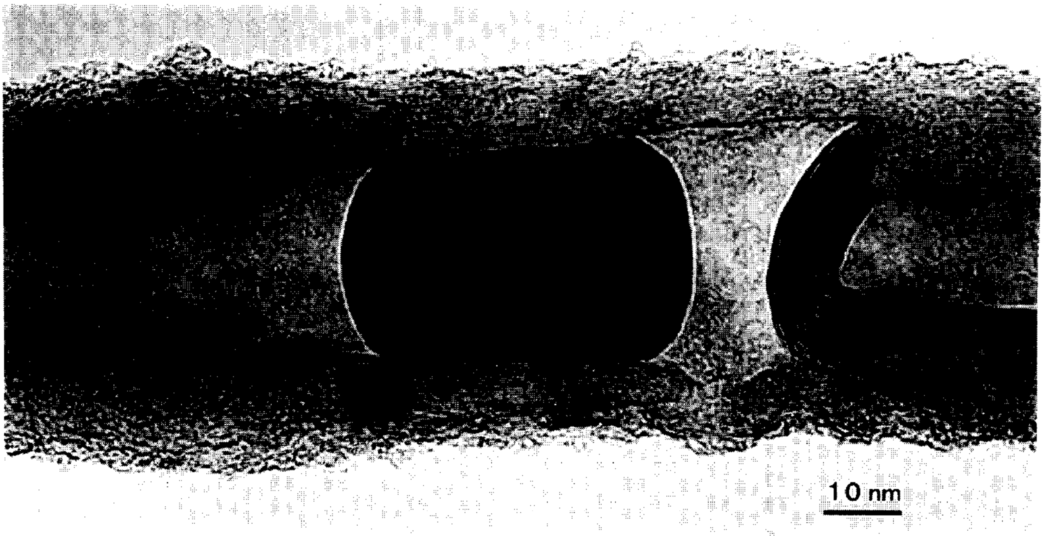

Fig. 10. TEM picture of a Ni metal left in the capillary of a graphite tube. Contact angle of the Ni particle on graphite surface (angle between the Ni/graphite interface and the Ni free surface) is larger than 90° (measured angle is about 140°), indicating poor wetting of Ni on the inner wall of a graphite tube.

methane is reportedly an indispensable ingredient to be added to an inactive gas (Ar for iron)[9]. For cobalt and nickel, on the other hand, no additives are necessary; the arc evaporation of metal-loaded graphite in a pure inactive gas (usually He) produces SW tubes. Figure 12 shows a TEM image of bundles of SW tubes growing radially from a Ni-carbide particle. The diameter of tubes are mostly in a range from 1.0 nm to 1.3 nm. Tips of SW tubes are capped and hollow inside. No contrast suggesting the presence of Ni clusters or particles is observed at the tips.

Effects of various combinations of 3*d*-transition metals on the formation of SW tubes have been studied by Seraphin and Zhou[41]. They reported that mixed metals enhanced the production of SW tubes; in particular, a 50% Fe + 50% Ni combination performed much better than Fe, Co, or Ni alone. It was also shown that the addition of some metals, such as Cu, to these metals poisoned their catalytic action.

Catalysts for SW tube formation are not confined to the iron-group metals. Some elements of the lanthanide series can catalyze the formation of SW tubes,

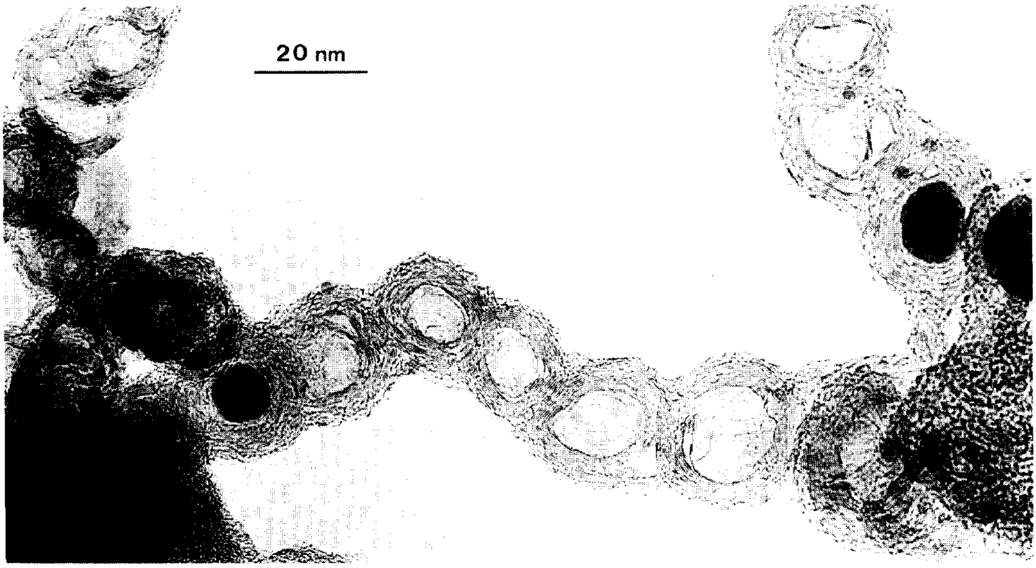

Fig. 11. TEM picture of nanochains.

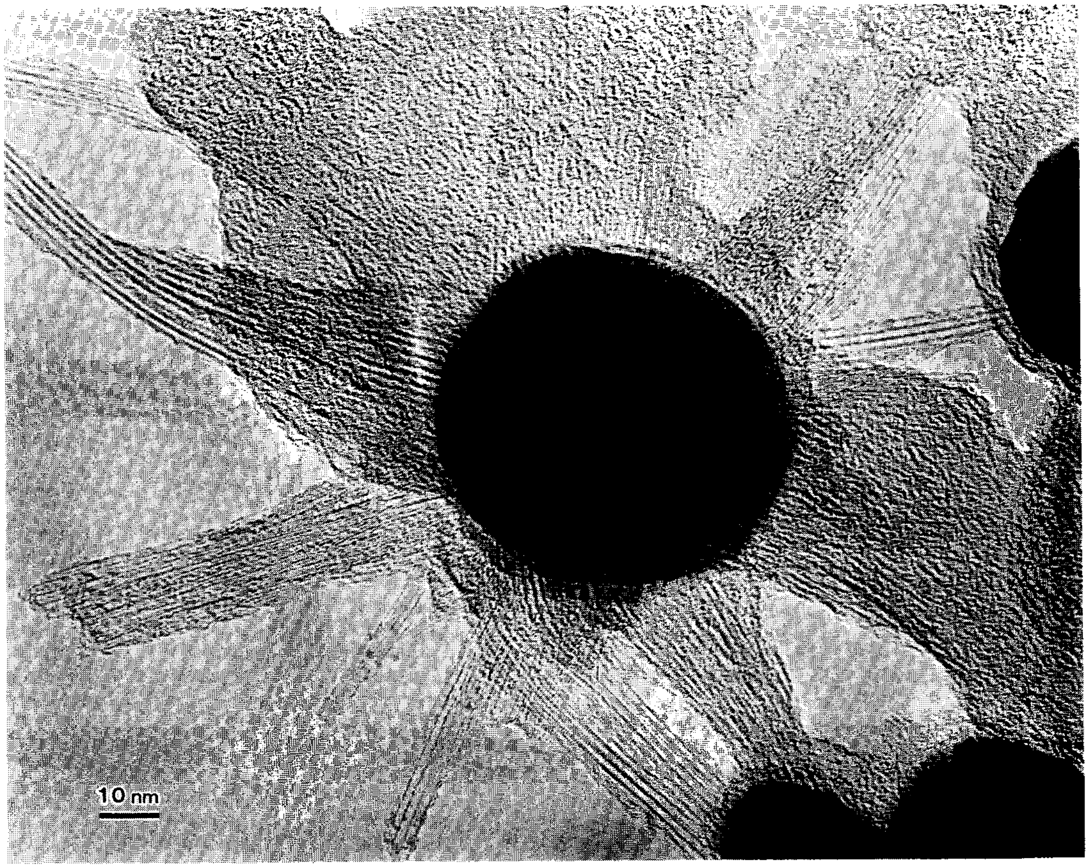

Fig. 12. TEM picture of single-wall tubes growing radially from a Ni-carbide particle.

as has been exemplified for Gd[42], Y[43], La[44] and Ce[45]. The morphology of the tubes that grow radially from these metal (or compound) particles and have "sea urchin"-like morphology is similar to that shown for Ni, but the length of tubes is shorter for the lanthanides (~100 nm long) than that of Ni (~μm long). The diameter of tubes produced from La is typically 1.8–2.1 nm, being larger (about twice) than that for Ni. It is reported that the addition of sulfur to Co catalyst promotes the formation of thicker SW tubes (in a range from 1 to 6 nm in diameter)[46]. The dependence of tube diameter on the catalysts employed suggests the possibility of producing SW tubes with any desirable diameter.

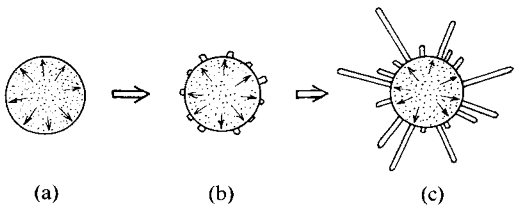

Fig. 13. Hypothetical growth process of SW tubes from a metal/carbon alloy particle: (a) segregation of carbon toward the surface, (b) nucleation of SW tubes on the particle surface and, (c) growth of the SW tubes.

A hypothetical growth process[40] of SW tubes from a core particle is illustrated in Fig. 13. When metal catalyst is evaporated together with carbon by arc discharge, carbon and metal atoms condense and form alloy (or binary mixed) particles. As the particles are cooled, carbon dissolved in the particles segregates onto the surface because the solubility of carbon decreases with the decrease of temperature. Some singular surface structures or compositions in an atomic scale may catalyze the formation of SW tubes. After the nuclei of SW tubes are formed, carbon may be supplied from the core particle to the roots of SW tubes, and the tubes grow longer, maintaining hollow capped tips. Addition of carbon atoms (and C_2) from the gas phase to the tips of the tubes may also help the growth of tubes.

4.3 *Anti-oxidation of wrapped iron nanocrystals*

The protective nature of graphitic carbon against oxidation of core nanocrystals was demonstrated by an environmental test (80°C, 85% relative humidity, 7 days)[44]. Even after this test, XRD profiles revealed that the capsulated iron particles were not oxidized at all, while naked iron particles with similar size, about 50 nm, were oxidized seriously to form oxides (rhombohedral-Fe_2O_3 and cubic-Fe_2O_3).

The magnetism of nanocrystallites contained in graphitic cages is intriguing, not only for scientific research, but also for applications such as magnetic fluids, magnetic ink, and so on.

REFERENCES

1. S. Iijima, *Nature* **354**, 56 (1991).
2. T. W. Ebbesen and P. M. Ajayan, *Nature* **358**, 220 (1992).
3. Y. Saito, T. Yoshikawa, M. Inagaki, M. Tomita, and T. Hayashi, *Chem. Phys. Lett.* **204**, 277 (1993).
4. Y. Chai, T. Guo, C. Jin, R. E. Haufler, L. P. F. Chibante, J. Fure, L. Wang, J. M. Alford, and R. E. Smalley, *J. Phys. Chem.* **95**, 7564 (1991).
5. H. Shinohara, H. Sato, M. Ohkohchi, Y. Ando, T. Kodama, T. Shida, T. Kato, and Y. Saito, *Nature* **357**, 52 (1992).
6. D. S. Bethune, R. D. Johnson, J. R. Salem, M. S. de Vries, and C. S. Yannoni, *Nature* **366**, 123 (1993).
7. R. S. Ruoff, D. C. Lorents, B. Chan, R. Malhotra, and S. Subramoney, *Science* **259**, 346 (1993).
8. M. Tomita, Y. Saito, and T. Hayashi, *Jpn. J. Appl. Phys.* **32**, L280 (1993).
9. S. Iijima and T. Ichihashi, *Nature* **363**, 603 (1993).
10. D. S. Bethune, C. H. Kiang, M. S. de Vries, G. Gorman, R. Savoy, J. Vazquez, and R. Beyers, *Nature* **363**, 605 (1993).
11. Y. Saito, T. Yoshikawa, M. Okuda, N. Fijimoto, K. Sumiyama, K. Suzuki, A. Kasuya, and Y. Nishina, *J. Phys. Chem. Solids* **54**, 1849 (1994).
12. Y. Saito, M. Okuda, T. Yoshikawa, A. Kasuya, and Y. Nishina, *J. Phys. Chem.* **98**, 6696 (1994).
13. M. Yoshida and E. Osawa, *Fullerene Sci. Tech.* **1**, 55 (1993).
14. Y. Saito, T. Yoshikawa, S. Bandow, M. Tomita, and T. Hayashi, *Phys. Rev. B* **48**, 1907 (1993).
15. M. S. Dresselhaus, G. Dresselhaus, K. Sugihara, I. L. Spain, and H. A. Goldberg, In *Graphite Fibers and Filaments*, p. 42. Springer-Verlag, Berlin (1988).
16. Y. Saito and M. Inagaki, *Jpn. J. Appl. Phys.* **32**, L954 (1993).
17. Y. Murooka and K. R. Hearne, *J. Appl. Phys.* **43**, 2656 (1972).
18. W. Finkelburg and S. M. Segal, *Phys. Rev.* **83**, 582 (1951).
19. D. R. McKenzie, D. Muller, and B. A. Pailthorpe, *Phys. Rev. Lett.* **67**, 773 (1991).
20. Pöttgen and W. Jeitschko, *Inorg. Chem.* **30**, 427 (1991).
21. Y. Saito, M. Okuda, T. Yoshikawa, S. Bandow, S. Yamamuro, K. Wakoh, K. Sumiyama, and K. Suzuki, *Jpn. J. Appl. Phys.* **33**, L186 (1994).
22. G. Adachi, N. Imanaka, and Z. Fuzhong, In *Handbook on the Physics & Chemistry of Rare Earths* (Edited by K. A. Gschneider, Jr. and L. Eyring) Vol. 15, Chap. 99, p. 61. Elsevier Science Publishers, Amsterdam (1991).
23. Y. Saito, T. Yoshikawa, M. Okuda, M. Ohkohchi, Y. Ando, A. Kasuya, and Y. Nishina, *Chem. Phys. Lett* **209**, 72 (1993).
24. R. E. Honig and D. A. Kramer, *RCA Rev.* **30**, 285 (1969).
25. H. Funasaka, K. Sugiyama, K. Yamamoto, and T. Takahashi, presented at 1993 Fall Meeting of Mat. Res. Soc., Boston, November 29 to December 3 (1993).
26. R. S. Ruoff, S. Subramoney, D. Lorents, and D. Keegan, presented at the 184th Meeting of the Electrochemical Society, New Orleans, October 10–15 (1993).
27. L. Moro, R. S. Ruoff, C. H. Becker, D. C. Lorents, and R. Malhotra, *J. Phys. Chem.* **97**, 6801 (1993).
28. Y. Saito, T. Yoshikawa, M. Okuda, N. Fijimoto, S. Yamamuro, K. Wakoh, K. Sumiyama, K. Suzuki,A. Kasuya, and Y. Nishina, *Chem. Phys. Lett.* **212**, 379 (1993).
29. T. Hihara, H. Onodera, K. Sumiyama, K. Suzuki, A. Kasuya, Y. Nishina, Y. Saito, T. Yoshikawa, and M. Okuda, *Jpn. J. Appl. Phys.* **33**, L24 (1994).
30. R. D. Heidenreich, W. M. Hess, and L. L. Ban, *J. Appl. Cryst.* **1**, 1 (1968).
31. T. Hihara, K. Sumiyama, K. Suzuki, to be submitted.
32. E. M. Brunsman, R. Sutton, E. Bortz, S. Kirkpatrick, K. Midelfort, J. Williams, P. Smith, M. E. McHenry, S. A. Majetich, J. O. Artman, M. De Graef, and S. W. Staley, *J. Appl. Phys.* **75**, 5882 (1994).
33. S. A. Majetich, J. O. Artman, M. E. McHenry, N. T. Nuhfe, and S. W. Staley, *Phys. Rev. B* **48**, 16845 (1993).
34. Y. Saito and T. Yoshikawa, *J. Cryst. Growth* **134**, 154 (1993).
35. A. Oberlin, M. Endo, and T. Koyama, *J. Cryst. Growth* **32**, 335 (1976).
36. M. R. Pederson and J. Q. Broughton, *Phys. Rev. Lett.* **69**, 2689 (1992).
37. P. M. Ajayan and S. Iijima, *Nature* **361**, 333 (1993).
38. T. W. Ebbesen, *Annu. Rev. Mater. Sci.* **24**, 235 (1994).
39. S. Seraphin, S. Wang, D. Zhou, and J. Jiao, *Chem. Phys. Lett.* **228**, 506 (1994).
40. Y. Saito, M. Okuda, N. Fujimoto, T. Yoshikawa, M. Tomita, and T. Hayashi, *Jpn. J. Appl. Phys.* **33**, L526 (1994).
41. S. Seraphin and D. Zhou, *Appl. Phys. Lett.* **64**, 2087 (1994).
42. S. Subramoney, R. S. Ruoff, D. C. Lorents, and R. Malhotra, *Nature* **366**, 637 (1993).
43. D. Zhou, S. Seraphin, and S. Wang, *Appl. Phys. Lett.* **65**, 1593 (1994).
44. Y. Saito, In *Recent Advances in the Chemistry and Physics of Fullerenes and Related Materials* (Edited by K. M. Kadish and R. S. Ruoff) p. 1419. Electrochemical Society, Pennington, NJ (1994).
45. Y. Saito, M. Okuda, and T. Koyama, *Surface Rev. Lett.*, to be published.
46. C. H. Kiang, W. A. Goddard, III, R. Beyers, J. R. Salem, and D. S. Bethune, *J. Phys. Chem.* **98**, 6612 (1994).
47. S. Bandow and Y. Saito, *Jpn. J. Appl. Phys.* **32**, L1677 (1993).
48. Y. Murakami, T. Shibata, T. Okuyama, T. Arai, H. Suematsu, and Y. Yoshida, *J. Phys. Chem. Solids* **54**, 1861 (1994).
49. D. Ugarte, *Chem. Phys. Lett.* **209**, 99 (1993).